

Combination of (M)DSC and surface analysis to study the phase behaviour and drug distribution of ternary solid dispersions

Joke Meeus¹, David J. Scurr², Xinyong Chen², Katie Amssoms³, Martyn C. Davies², Clive J. Roberts², Guy Van den Mooter¹

¹Drug Delivery and Disposition, KU Leuven, Leuven, Belgium

²Laboratory of Biophysics and Surface Analysis, School of Pharmacy, The University of Nottingham, Nottingham, United Kingdom

³Pharmaceutical Companies of Johnson & Johnson, Janssen, Discovery Sciences, PD&S_PDM, Beerse, Belgium

* Corresponding author. Drug Delivery and Disposition, KU Leuven, Department of Pharmaceutical and Pharmacological Sciences, Campus Gasthuisberg ON2, Herestraat 49 b921, 3000 Leuven, Belgium. Tel.: +32 16 330 304, Fax: +32 16 330 305, e-mail: guy.vandenmooter@pharm.kuleuven.be

ABSTRACT

Purpose: Miscibility of the different compounds that make up a solid dispersion based formulation play a crucial role in the drug release profile and physical stability of the solid dispersion as it defines the phase behaviour of the dispersion. The standard technique to obtain information on phase behaviour of a sample is (modulated) differential scanning calorimetry ((M)DSC). However, for ternary mixtures (M)DSC alone is not sufficient to characterize their phase behaviour and to gain insight into the distribution of the active pharmaceutical ingredient (API) in a two-phased polymeric matrix.

Methods: MDSC was combined with complementary surface analysis techniques, specifically time-of-flight secondary ion mass spectrometry (ToF-SIMS) and atomic force microscopy (AFM). Three spray-dried model formulations with varying API/PLGA/PVP ratios were analyzed.

Results: The distribution of the API in the ternary solid dispersions depended on formulation parameters. The extent of API surface coverage and therefore the distribution of the API over both polymeric phases differed significantly for the three formulations.

Conclusions: Combining (M)DSC and surface analysis rendered additional insights in the composition of mixed phases in complex systems, like ternary solid dispersions.

ABBREVIATIONS

AFM	atomic force microscopy
API	active pharmaceutical ingredient
DDS	drug delivery system
(M)DSC	(modulated) differential scanning calorimetry
HIV	human immunodeficiency virus
PLGA	poly(lactic-co-glycolic acid)
PVP	polyvinylpyrrolidone
T_g	glass transition temperature
ToF-SIMS	time of flight secondary ion mass spectrometry

INTRODUCTION

Solid dispersions are an intensively investigated enabling technology to formulate poorly soluble drugs so as to improve their bioavailability (1–5). Phase behaviour of the different compounds plays a crucial role in this type of formulation as it will determine whether a given drug-polymer combination will be present as a glass solution (molecular dispersion) or a phase separated system (amorphous-amorphous or amorphous-crystalline phase separation). Hence, the phase behaviour will have an influence on the release profile and stability performance of such a formulation. The technique of (Modulated) differential scanning calorimetry ((M)DSC) is generally used to study the phase behaviour and miscibility of a drug delivery system (DDS). Based upon the experimentally observed glass transition temperatures (T_g s) the phase behaviour and composition of binary drug-polymer mixtures can be estimated by a number of expressions such as the Gordon-Taylor, Fox or Couchman-Karasz equation. All of these equations are mathematical derivations on the same theme and were originally developed for ideal binary polymer systems (6). For binary pharmaceutical samples the Gordon-Taylor equation is the most frequently used expression to describe the relationship between the T_g and sample composition (7). A similar expression for ternary mixtures has been developed but finds limited application due to the contradiction between the complexity of ternary mixtures and the assumptions made for this model equation (6). Therefore for ternary mixtures (M)DSC alone is not sufficient to characterize the composition of the different phases present, as for a mixed phase it is virtually impossible to determine the weight fraction of each of the three compounds. Knowledge of the composition of the different phases would inform on the distribution of a drug throughout the DDS. Inhomogeneous drug distribution, such as surface enrichment, can only be detected by comparing the bulk characteristics of that formulation to its surface properties, indicating the need of surface analysis for ternary solid dispersions.

Information on both phase behaviour and spatial drug distribution is indispensable as these characteristics can be decisive for the release characteristics of a solid dispersion. For example, phase behaviour might influence the release, as particles containing a poorly soluble drug in the form of amorphous precipitates in the polymeric matrix are likely to have a slower release compared to ideal glass solutions where the drug is molecularly dispersed within a matrix. Spatial drug distribution might also influence the performance of a solid dispersion. For instance, enrichment of drug at the surface results in an increased size or number of (amorphous) drug domains at the surface. This jeopardizes the increased solubility originating from the (molecular) dispersion of the poorly soluble drug. In that way surface-bulk distribution of the drug will determine the release kinetics of the sample. Additionally surface enrichment of an amorphous drug makes the solid dispersion more prone to surface crystallization and therefore might be detrimental to its stability. These issues highlight why surface characterization of solid dispersions is crucial in understanding how they perform with respect to dissolution and stability.

We have previously reported on the development of spray-dried polymeric microspheres for intramuscular injection for the long-term prophylaxis of infection with human immunodeficiency virus (HIV) (8,9). These shell structured microspheres contain two biocompatible polymers, poly(lactic-co-glycolic acid) (PLGA) and polyvinylpyrrolidone (PVP) and are made up of a PLGA-rich surface layer and an underlying PVP-rich phase (8). MDSC analysis revealed, based upon the Gordon-Taylor equation, that the polymeric microspheres are estimated to consist of a PLGA-rich surface phase (85% PLGA, 15% PVP) and a PVP-rich underlying phase (97% PVP, 3% PLGA) (9).

For the present study a poorly soluble active pharmaceutical ingredient (API) was dispersed in these microspheres as a solid dispersion. The model drug used was an HIV protease inhibitor. Three model formulations with varying ratios of API/PLGA/PVP were developed. As mentioned above, after inclusion of the API the composition of the mixed phases cannot be determined by (M)DSC. To discern the distribution of the API in the microspheres and thus the ternary solid dispersions, (M)DSC was combined with surface analysis techniques, namely ToF-SIMS and AFM. The potential of this combination lies in the complementarity of the techniques. (M)DSC is a bulk thermo-analytical technique, whereas ToF-SIMS is a surface mass spectrometry technique capable of analyzing the top 1-2 nm. AFM enables spatial characterization of topographic and mechanical properties of a sample surface at nanoscale resolution.

For ToF-SIMS analysis, chemical identification of different compounds at the sample surface is based upon the detection of secondary ions, including molecular species or fragments derived from these compounds. Besides chemical identification, this technique can also provide information on spatial distribution of compounds at the sample surface via ToF-SIMS chemical imaging. The utility of ToF-SIMS for the analysis of solid dispersions lies mainly in its potential to reveal the spatial distribution of drug and excipient at the sample surface (9–12). Evidently, this information is indispensable for complete characterization of solid dispersions. Homogeneous mixing, at least at the resolution of the ToF-SIMS data (on the order of microns) is assessed by uniformity of the drug and polymer distribution at the sample surface.

The main contribution of AFM for the analysis of solid dispersions lies in its potential to spatially resolve the phase separation at nanoscale resolution (9,13–16). Although this

technique is not yet that frequently used for the characterization of pharmaceutical samples, it exhibits great potential as various mechanical properties (eg. stiffness, adhesion and friction) can be monitored to distinguish different compounds.

This study aims to clarify drug distribution in a multi-phased polymeric system. To do so, for the first time, (M)DSC was combined with ToF-SIMS and AFM to characterize the phase behaviour of ternary solid dispersions.

MATERIALS AND MATHODS

Materials

Poly(lactic-co-glycolic acid) (PLGA) (lactide:glycolide molar ratio of 75:25, inherent viscosity of 0.2 dl/g) was purchased from PURAC Biomaterials (Gorinchem, The Netherlands). Polyvinylpyrrolidone K30 (PVP K30) (MW 44-54 kDa) was kindly donated by BASF (Ludwigshafen, Germany). The API was a poorly soluble HIV protease inhibitor provided by Janssen (Beerse, Belgium) and its structure is shown in Figure 1. Dichloromethane (DCM) was provided by Fisher Scientific (Leicestershire, United Kingdom).

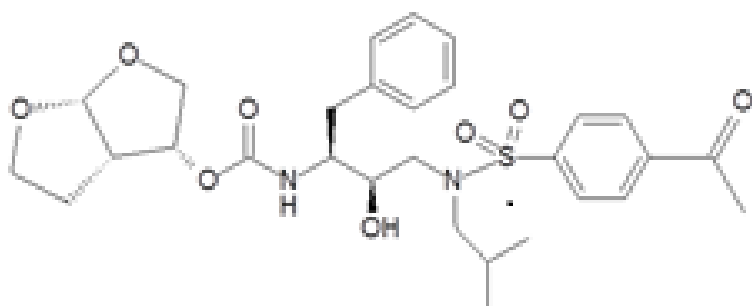


FIGURE 1 Structural formula of the API, a poorly soluble HIV protease inhibitor.

Methods

Spray drying

Three model ternary solid dispersions made up of API, PLGA and PVP were prepared by spray drying and had the following composition: 10/75/15, 20/50/30 and 30/25/45 wt% API/PLGA/PVP. Samples were spray dried with a Micro Spray lab scale spray dryer (ProCepT, Zelzate, Belgium) starting from a 5% feed solution in dichloromethane (DCM). The inlet temperature was set to 115°C and the feed rate was 6 mL/min. The co-current drying air had a flow rate of 0.2 m³/min and the atomizing air was supplied with a pressure of 1.25 bar.

Modulated differential scanning calorimetry

The bulk miscibility behaviour of the spray-dried microspheres was determined by MDSC (Q2000, TA Instruments, Leatherhead, UK). Thermal Analysis Software (Version 4.4A) was used to analyze the obtained data. Crimped aluminum pans (TA Instruments, Brussels, Belgium) were selected for the analysis of the samples. An empty pan was used as a reference and the masses of the reference pan and of the sample pans were taken into account. The DSC cell was purged with a nitrogen flow rate of 50 mL/min.

Indium and octadecane were chosen for temperature calibration. The enthalpic response was calibrated with indium. The modulation parameters used were a heating rate of 1°C/min, a period of 40 s and an amplitude of 1°C. Calibration of the heat capacity was done using sapphire. Samples were analyzed from -20°C to 220°C. Glass transitions were analyzed in the reversing heat flow signals.

Scanning electron microscopy

SEM was used to study the morphology and particle size of the samples which were prepared by fixing an amount of powder on an aluminum stub using double-sided carbon tape. The samples were coated with a gold-palladium mixture by sputtering for 45 s at 20 mA. Field emission gun scanning electron micrographs (FEG-SEM) were taken by using a Philips XL30 ESEM-FEG instrument (Philips, Eindhoven, The Netherlands) at an acceleration voltage of 10 kV.

Time-of-flight secondary ion mass spectrometry

Spray-dried samples were adhered to double-sided adhesive tape in order to produce an immobile surface suitable for ToF-SIMS analysis. The data were acquired using a ToF-SIMS IV instrument (ION-TOF GmbH) equipped with a bismuth liquid metal ion gun and a single-stage reflectron analyzer. Typical operating conditions utilised a 25 kV Bi_3^+ primary ion source with a pulsed target current of approximately 0.3 pA. A flood gun producing low energy electrons (20 eV) was used to compensate for surface charging caused by the positively charged primary ion beam on the insulating sample surface. A 4 mm \times 4 mm area of each sample was raster scanned at a resolution of 100 pixels per mm. PLGA and PVP were identified using $\text{C}_6\text{H}_7\text{O}_4^-$ ($m/z = 143$), and $\text{C}_5\text{H}_8\text{O}^-$ ($m/z = 84$) respectively. The API was characterized by $\text{C}_8\text{H}_7\text{SO}_3^-$ ($m/z = 183$). Prior to sample analysis, reference materials were analyzed and the characteristic ion peaks $\text{C}_6\text{H}_7\text{O}_4^-$, $\text{C}_5\text{H}_8\text{O}^-$ and $\text{C}_8\text{H}_7\text{SO}_3^-$ were selected and only present in PLGA, PVP and API respectively. Negative polarity ToF-SIMS spectra showing the markers for API, PLGA and PVP are shown in Figure 1 of the Supplementary Information. Static conditions were ensured by keeping the total primary ion beam dose for every analyzed area below 1×10^{12} ions/cm² throughout the analysis. Data in the negative secondary ion polarities were collected and analyzed using SurfaceLab 6 software (IONTOF). For any given sample, the measured secondary ion intensity for each polymer and API marker

peak was normalized to the total intensity count to enable a semi-quantitative comparison of the different samples.

Atomic force microscopy

The spray-dried powders were applied onto a fresh mica surface using a Gilson pipette tip, and slightly blown with pressured nitrogen gas. Freshly cleaved mica (Agar Scientific, Stansted, U.K.) was used as sample substrate. Samples were imaged with a Bruker Dimension FastScan Bio AFM in PeakForce Quantitative Nano-Mechanics (QNM) mode (Bruker UK Ltd, Coventry, UK). Tap150A (also called as MPP-12120, Bruker) tips (5 N/m, 150 kHz, rotated tip, aluminum reflective coating) were used for Peak Force imaging.

PeakForce QNM is a novel development in AFM techniques. Whilst the tip is driven oscillated at its resonant frequency in the traditional Tapping mode, the tip taps the sample surface at a frequency substantially lower than its resonant frequency in PeakForce mode, for example, 2 kHz vs 150 kHz in the present case. The vertical position of the AFM tip is maintained under continuous active control allowing an accurate constant maximum contact force whilst maintain nanoscale spatial resolution (17). The active cantilever control allows a simultaneous extraction of quantitative information related to surface properties such as stiffness and adhesion alongside the traditional topographic data (18). To calculate sample stiffness from the tip-sample interaction force data the Hertzian based DMT (Derjaguin-Muller-Toporov) model was applied which assumes the contact is between a rigid sphere (the silicon AFM tip apex) and a soft flat surface (the polymeric microparticle). Gwyddion software (version 2.22) was used for data analysis.

RESULTS

Morphological characterization of microspheres

The particle size and surface morphology of the microspheres of the different formulations were compared via SEM. Although a statistically significant number of particles were not analyzed, SEM could be used as an indicator for both particle size and morphology. Figure 2 shows that there are no striking differences regarding particle size and morphology when comparing the three model formulations. Particles are spherical, with a smooth, intact surface and an estimated diameter approximately between 1 μm and 7 μm .

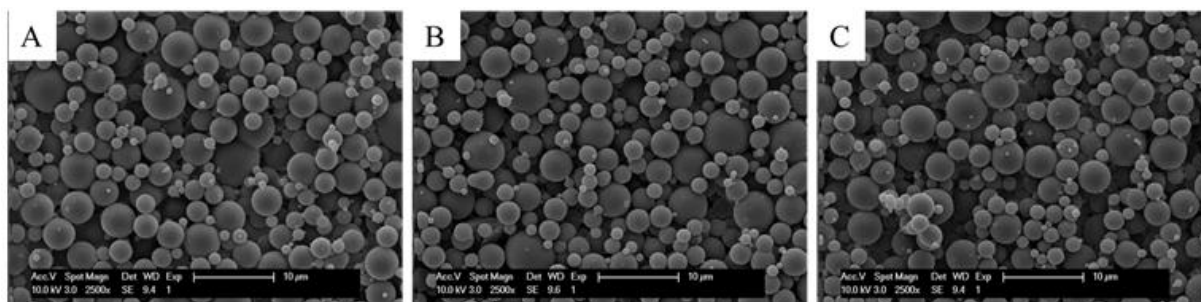


FIGURE 2 Scanning electron micrographs of the model formulations with following API/PLGA/PVP (w/w/w) ratios: (a). 10/75/15, (b). 20/50/30 and (c). 30/25/45.

Phase behaviour

MDSC was used to determine the T_g s of the pure compounds, which were 38°C for PLGA, 56°C for the API and 174°C for PVP under the given experimental conditions. The phase behaviour of the model formulations was examined and the resulting thermograms are displayed in Figure 3. For each sample two mixing T_g s were observed, the first one approximating to the T_g of PLGA and the second one shifting towards the T_g of pure PVP (Fig. 3). The known T_g of the API (around 56°C) was not observed in the thermograms.

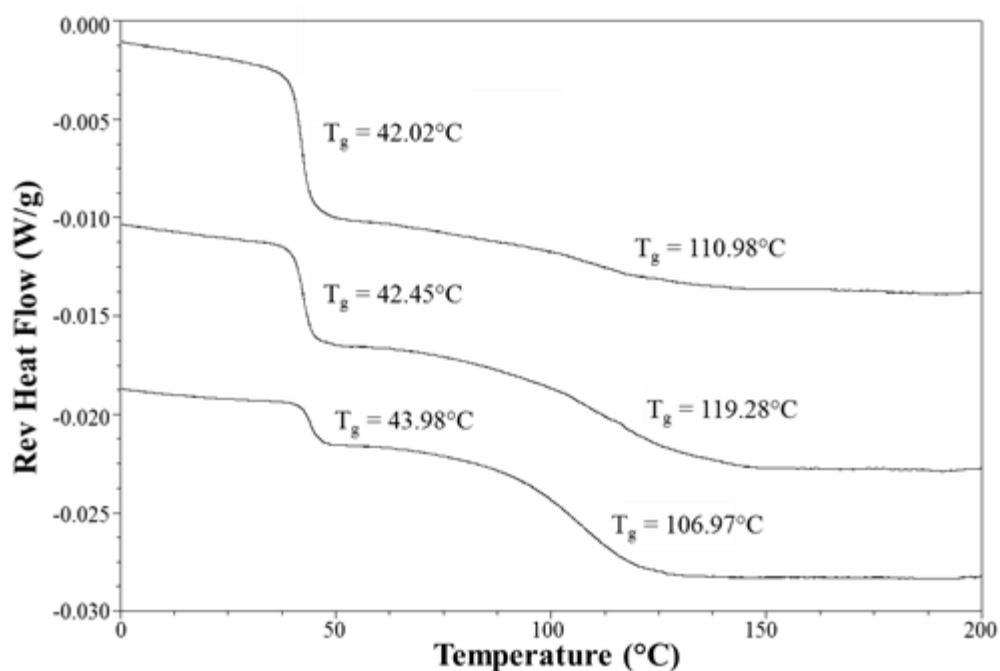


FIGURE 3 MDSC of the model formulations. From top to bottom reversing heat flow with following API/PLGA/PVP (w/w/w) ratios: (a). 10/75/15, (b). 20/50/30 and (c). 30/25/45.

Surface chemical analysis

ToF-SIMS was used to chemically analyze the surfaces of the microspheres and hence solid dispersions. The spatial distribution of the API and PLGA at the sample surface is represented in Figure 4. There is a negligible amount of PVP observed at the particle surface which is consistent with previous studies (8,9) and depicted in Figure 2 of the Supplementary Information. At the micron-scale resolution of the ToF-SIMS data the drug seems to be homogeneously distributed at the surface of the three model formulations. For the formulation containing 20 wt% API a significantly higher intensity for the marker of the API is observed.

Figure 5 illustrates the measured API intensity at the sample surface and hence depicts a measure of API surface coverage for the three model formulations. Ranking of the formulations based upon the observed API surface coverage is as follows: 30/25/45 < 10/75/15 < 20/50/30 API/PLGA/PVP wt%, whereas ranking based upon total API content is:

30/25/45 < 20/50/30 < 10/75/15 API/PLGA/PVP wt%. Hence the appearance of API at the particle surface is not in agreement with the total amount of API present in the microparticles, e.g. formulation 30/25/45 API/PLGA/PVP wt% has the highest bulk concentration of API (30 wt%) but shows the lowest surface coverage compared to the other model formulations.

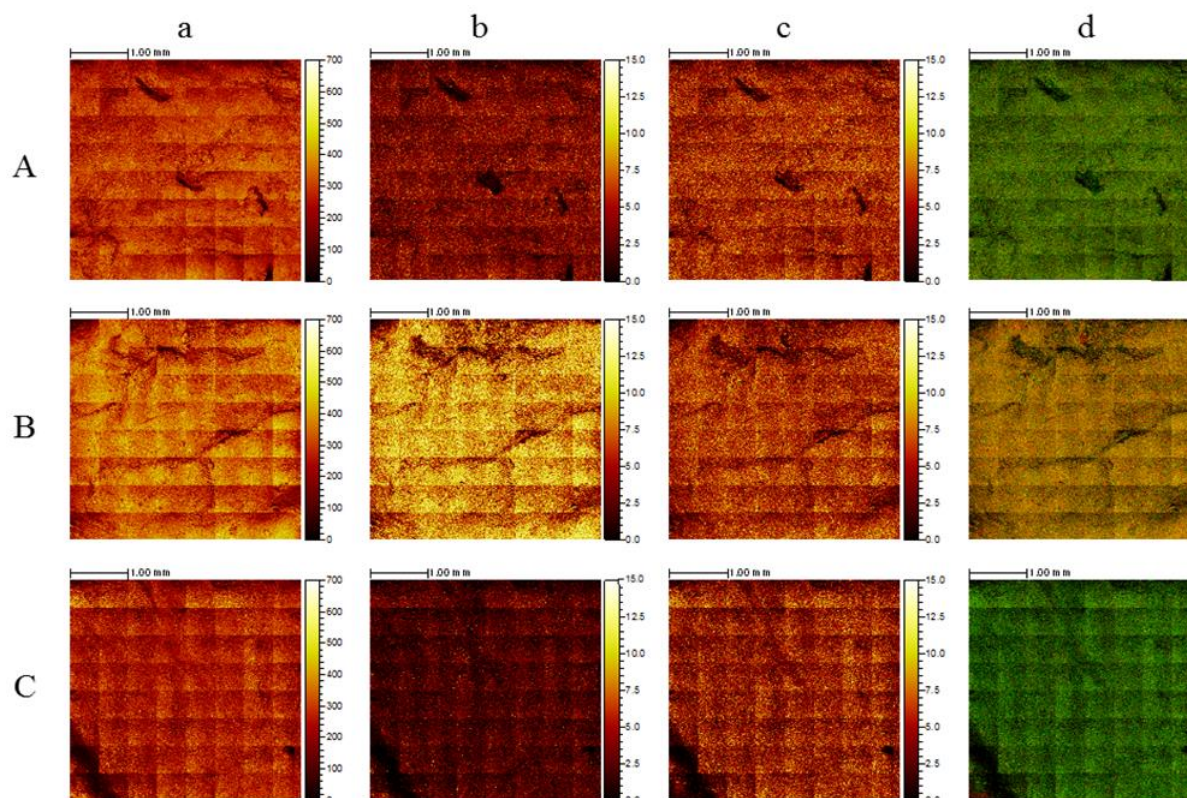


FIGURE 4 ToF-SIMS secondary ion intensity images of the model formulations with the following API/PLGA/PVP (w/w/w) ratios: (a). 10/75/15, (b). 20/50/30, (c). 30/25/45. Panels a show results of the total intensity signal. Panels b and c show negative polarity images of respectively API ($m/z=183$) and PLGA ($m/z=142$). Panels d show the negative polarity overlay images (PVP in red, PLGA in green) (4 mm×4 mm scan size).

Surface topographical analysis

Simultaneous mapping of topography and surface properties using QNM in PeakForce mode revealed the surface structure of the three formulations. Figures 6-8 show topography (3D and 2D views) along with the corresponding stiffness map for the microspheres of the 10/75/15,

20/50/30 and 30/25/45 API/PLGA/PVP wt% samples. The 3D data emphasize that these images are acquired from the apex of immobilized microspheres. The 2D representation following the background subtraction of the image curvature reveals surface structure in details. For the 10 wt% and 30 wt% API samples little surface topographic variation is observed with a smooth homogeneous surface evident (Fig. 6A-B, Fig. 8A-B). The 20 wt% API sample shows significant heterogeneity in surface topography (Fig. 7A-B). Similarly the corresponding stiffness maps only show significant heterogeneity in the 20 wt% API sample (Fig. 6C, 7C, 8C).

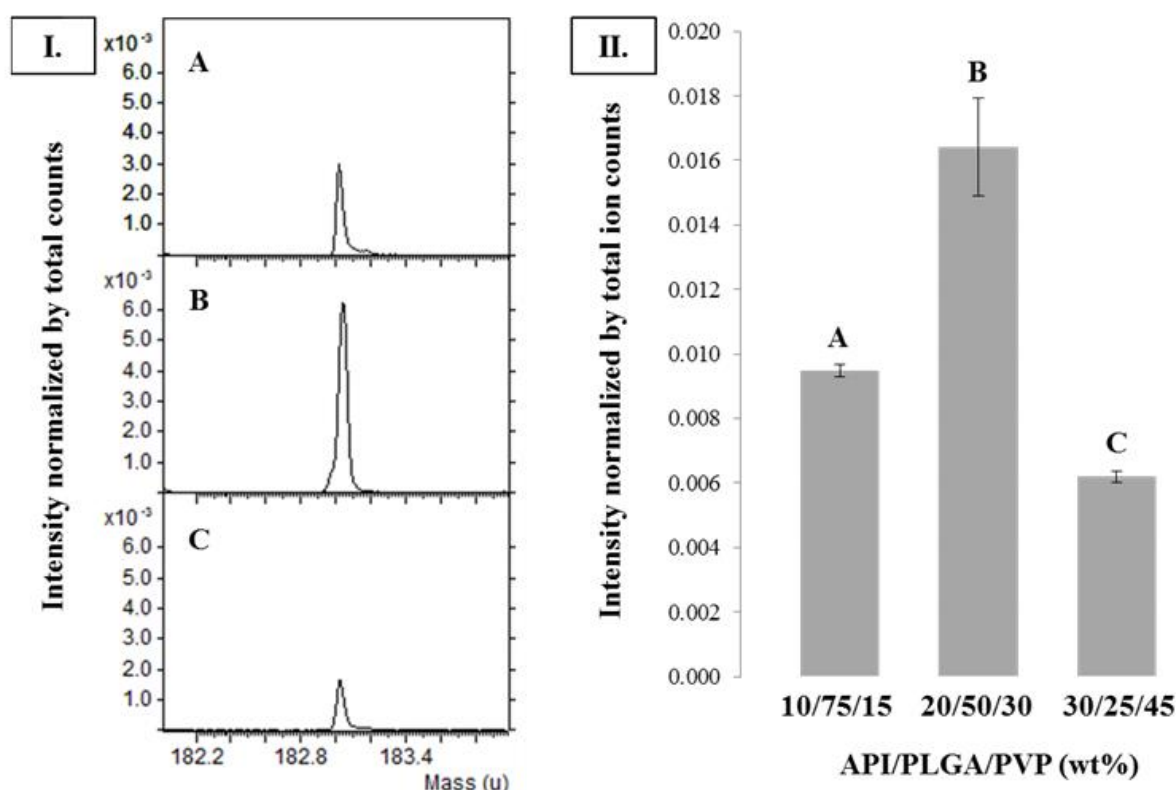


FIGURE 5 I. Negative ToF-SIMS spectra at m/z 183 (marker API) of the model formulations with the following API/PLGA/PVP (w/w/w) ratios: (a). 10/75/15, (b). 20/50/30, (c). 30/25/45. II. Histogram representing the intensity at m/z 183 for the three model formulations (1 mm×1 mm scan size, n=4).

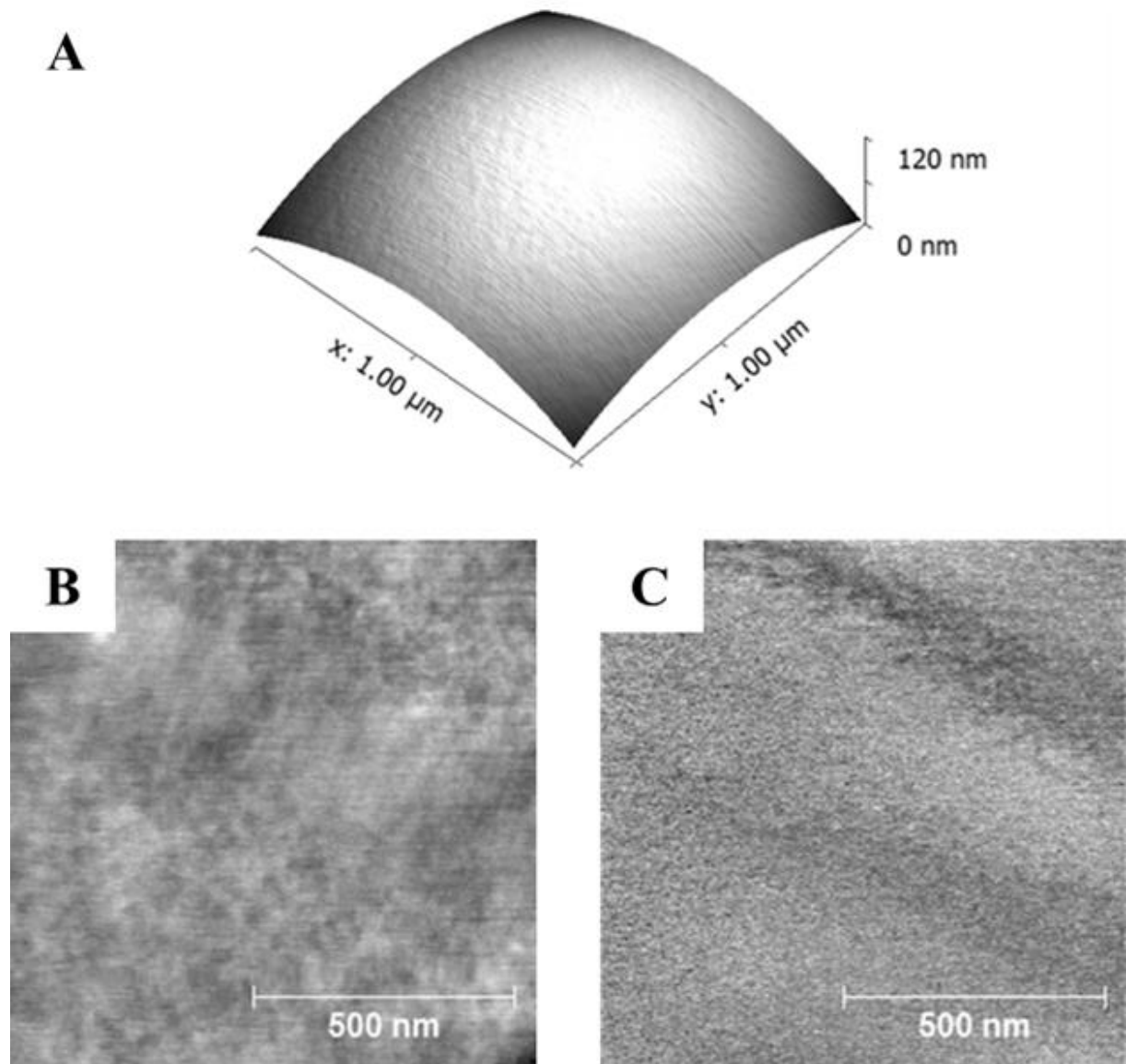


FIGURE 6 Peak Force QNM AFM analysis of a spray-dried 10/75/15 API/PLGA/PVP particle. (a). 3D representation of the AFM topographic data showing a region of the particle displaying a smooth featureless surface, (b). 2D representation of the topographic data (following flattening of the data (vertical grey scale 4 nm)) and (c). a corresponding sample stiffness map (based upon DMT analysis, lighter being stiffer (arbitrary scale)).

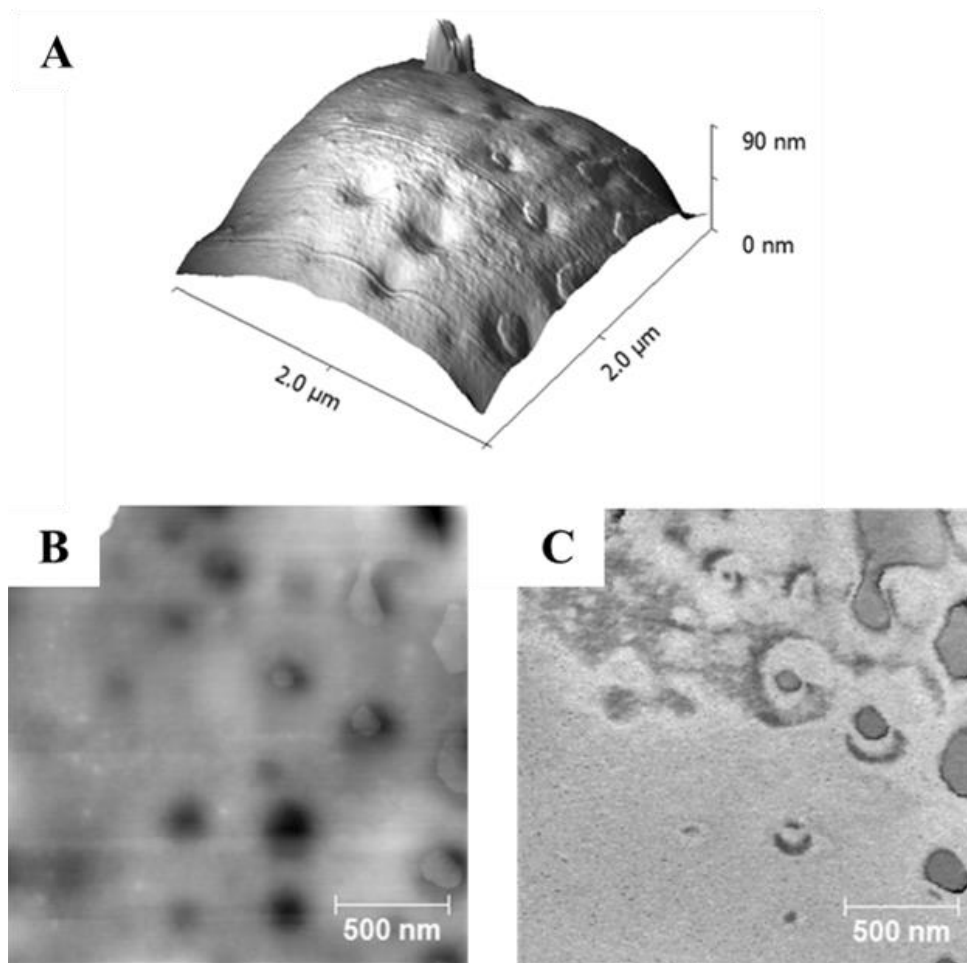


FIGURE 7 Peak Force QNM AFM analysis of a spray-dried 20/50/30

API/PLGA/PVP particle. (a). 3D representation of the AFM topographic data showing a region of the particle displaying clear heterogeneity including surface depressions, (b). 2D representation of the topographic data (following flattening of the data (vertical grey scale 30 nm)) and (c). a corresponding sample stiffness map (based upon DMT analysis, lighter being stiffer (arbitrary scale)).

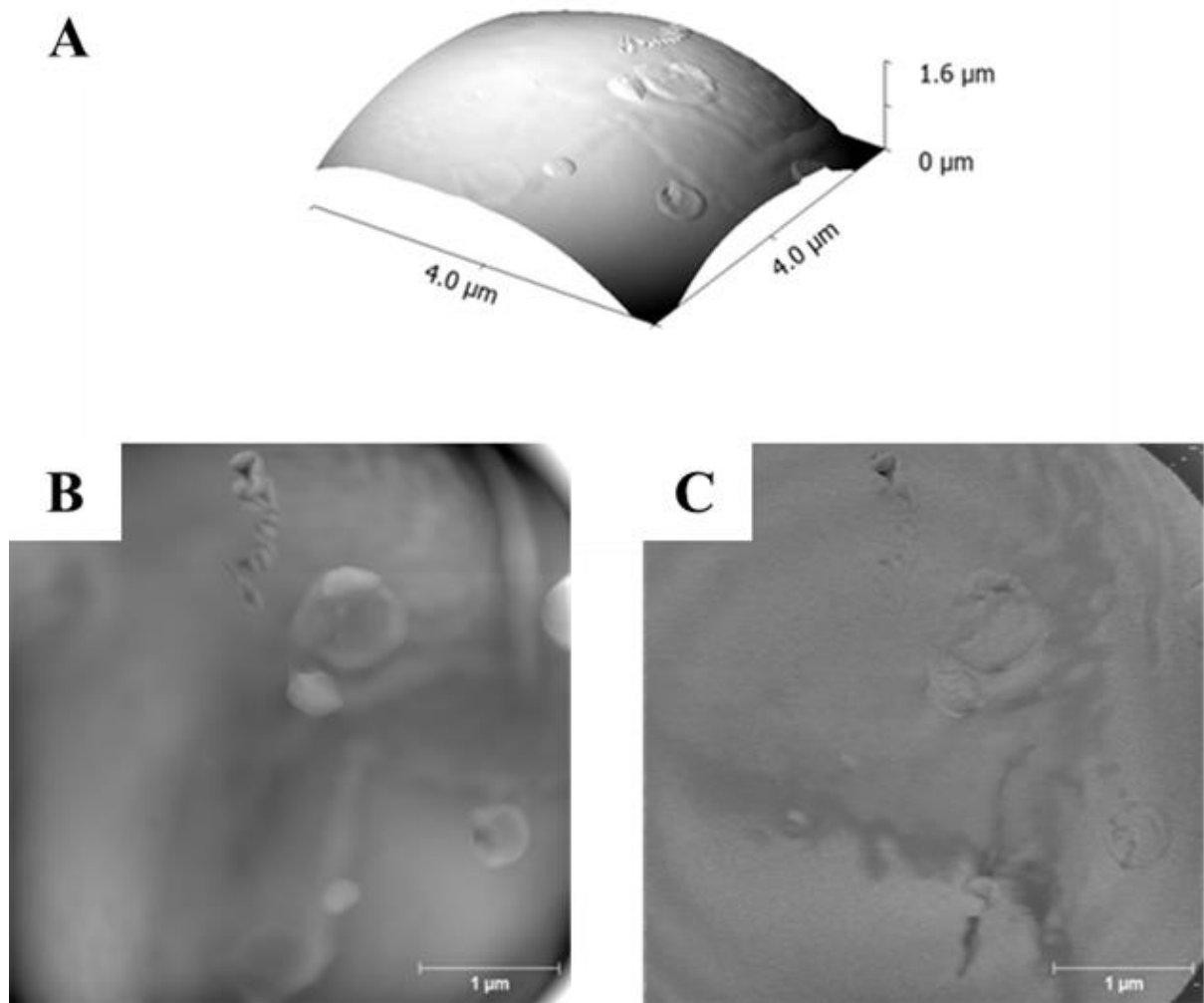


FIGURE 8 Peak Force QNM AFM analysis of a spray-dried 30/25/45 API/PLGA/PVP particle. (a). 3D representation of the AFM topographic data showing a region of the particle displaying a relatively smooth surface with some circular features, (b). 2D representation of the topographic data (following flattening of the data (vertical grey scale 300 nm)) and (c). a corresponding sample stiffness map (based upon DMT analysis, lighter being stiffer (arbitrary scale)). Note the small triangular indents at the top of the image are due to a high force threshold during the AFM tip's raw engagement.

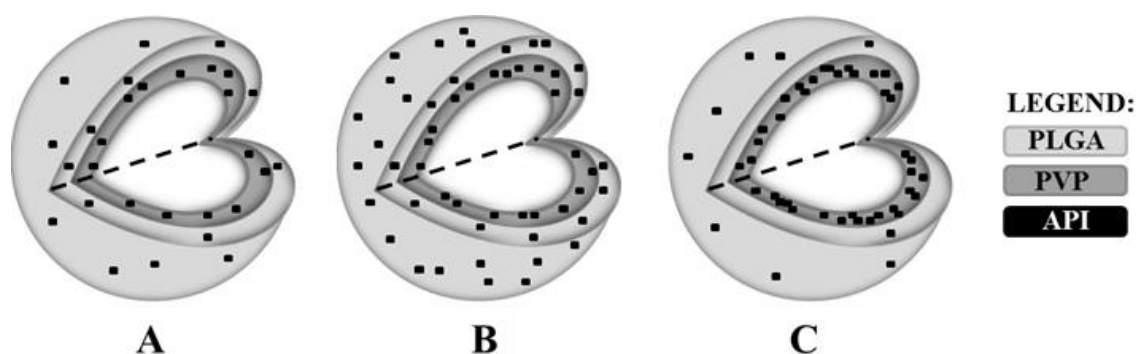


FIGURE 9 Elucidated structures of the model formulations with following API/PLGA/PVP (w/w/w) ratios: (a). 10/75/15, (b). 20/50/30 and (c). 30/25/45.

DISCUSSION

MDSC was used to thermally study the phase behaviour of the three model formulations. For each sample two mixing T_g s were observed, the first one approximating to the T_g of PLGA and the second one shifting towards the T_g of pure PVP (Fig. 3). In addition, the absence of a T_g around 56°C (T_g of the API) indicates that the API is molecularly dispersed in a phase separated system made up of a PLGA-rich phase and a PVP-rich phase. Preceding work has already revealed that hollow spheres are formed when PLGA and PVP are spray-dried together with a PLGA surface layer and an underlying PVP layer (8,9). The presence of PLGA at the particle surface is due to its surface activity and a consequence of restructuring of the methyl side groups of PLGA towards the droplet-air surface (8,19). Moreover these two polymeric phases display a small degree of miscibility which is determined by the PLGA to PVP ratio (8). The additional presence of an API will influence this phase behaviour.

Phase behaviour of the polymeric PLGA/PVP matrix was studied by estimating the polymer miscibility in these binary systems based upon the observed T_g s using the Gordon-Taylor equation for binary mixtures (equation 1) (7).

$$T_{gmix} = (w_1T_{g1} + Kw_2T_{g2}) / (w_1 + Kw_2) \quad (1)$$

In this equation, the weight fraction of each compound is represented by w , the glass transition temperature by T_g and the subscripts 1 and 2 represent the compounds with the lowest and the highest glass transition temperatures respectively. The constant K can be assessed by using the Simha-Boyer rule (equation 2), with ρ being the density of the amorphous compounds.

$$K \approx (\rho_1 T_{g1}) / (\rho_2 T_{g2}) \quad (2)$$

Consequently the amount of PVP present in the PLGA layer and the amount of PLGA present in the PVP layer could be calculated. The PVP content in the PLGA phase was thus estimated to be 15% and the PLGA content in the PVP phase 3% (9).

The complex phase behaviour of ternary, or even quaternary (when taking residual solvent into account), systems is however difficult, if not impossible to assess using this equation. An extended form of the Gordon-Taylor equation for ternary mixtures has been developed (equation 3).

$$T_{gmix} = (w_1 T_{g1} + K_1 w_2 T_{g2} + K_2 w_3 T_{g3}) / (w_1 + K_1 w_2 + K_2 w_3) \quad (3)$$

With w representing the weight fraction of each compound, T_g the glass transition where the subscripts 1, 2 and 3 represent the compounds with the lowest, middle and the highest glass transition temperatures, respectively. The constants K_1 and K_2 are analogously obtained by equation 2.

This extended formula was originally used to account for residual (plasticizing) solvent (20–22) and was expanded to the analysis of ternary solid dispersions (23). However, this extended form finds limited application due to the contradiction between the complexity of ternary mixtures and the assumptions made for this model equation. Generally the Gordon-Taylor equation assumes additivity of the specific volumes of the compounds involved as well as a linear change in volume with temperature (6). Obviously the likelihood that those assumptions apply decreases with increasing complexity of the system.

Illustratively equation 3 was applied to the observed T_g of the PLGA-rich phase of the 20/50/30 API/PLGA/PVP wt% sample ($T_g = 42.45^\circ\text{C}$). Assuming ideal mixing of this ternary system, the calculated amount of API could vary between 0 and 10 wt% API in the PLGA-rich phase. This variation in composition might be translated to differences in the release profile and physical stability of the formulation. The above indicates that (M)DSC alone does not allow the determination of the ternary composition of the two phases present and is not sufficient to characterize these complex ternary system samples as it is unable to inform on the distribution of the API in the PLGA-rich surface layer and the underlying PVP-rich phase. Owing to this limitation, for these systems MDSC must be applied in combination with surface analysis in order to determine the composition.

ToF-SIMS was utilised to chemically elucidate the surface composition of the microspheres of the different formulations. Chemical surface analysis by ToF-SIMS revealed that the degree of API surface coverage of the solid dispersion clearly differed when formulation parameters were changed (Fig. 4-5). Additionally, an inconsistency was observed between the API bulk concentration and surface coverage. The sample with the highest total amount of API (30/25/45 API/PLGA/PVP wt%) did not show the highest amount of API present at the

surface, in fact it displayed the lowest surface coverage. This discrepancy indicates that the API distribution of the drug is influenced by formulation parameters. The observed susceptibility of these systems regarding API distribution induced by changes in formulation (and likely process) parameters indicates the need for in depth sample characterization, combining miscibility, characterization of API surface coverage and spatial API distribution at higher resolution.

AFM imaging of the three samples showed identifiable differences between the appearance and organization of the formulations. In general, spray-dried particles of the 10/75/15 API/PLGA/PVP wt% formulation showed a smooth featureless topography with no evidence of sample heterogeneity. Corresponding surface stiffness maps also indicated a homogenous material with no significant nanoscale variation in mechanical properties (Fig. 6). Similar observations were also made for the 30/25/45 API/PLGA/PVP wt% samples. Although particles did show some circular topographic features no significant variation in mechanical properties was observed (Fig 8), again indicating a compositionally homogeneous surface. In contrast, the 20/50/30 API/PLGA/PVP wt% formulation showed some significant heterogeneity in its surface topography and composition. There is clear evidence of pits in the surface of the order of hundreds of nanometers in diameter and 2-15 nm in depth. The stiffness map shows areas of reduced stiffness (darker contrast) in relation to the majority of the surface, sometimes but not always associated with the pits (Fig. 7). Whilst AFM does not uniquely (chemically) identify components as in ToF-SIMS the observation of complexity at the surface of the 20/50/30 as compared to the 10/75/15 and 30/25/45 API/PLGA/PVP wt% samples is consistent with the 20 wt% API samples showing a higher than expected ratio of API at the surface of the particles. The AFM indicates that the structural pits may be revealing

underlying material that contains API and/or that surface heterogeneity (incomplete mixing of components) in these samples is related to the higher API surface coverage.

The information regarding the phase behaviour of the polymers obtained by MDSC was combined with the information ToF-SIMS provided on the spatial distribution of the API at the surface of the microspheres as well as on the ranking of the formulations based on API surface coverage. AFM provided spatial information on the distribution of different compounds at the microsphere surface at nanoscale resolution. Taken together these techniques provide insights into differences in drug distribution (via the observed surface coverage) for three differently composed ternary solid dispersions. A schematic illustration of the elucidated structures of the three model formulations is shown in Figure 9.

The observed differences between the formulations studied can be explained by the fact that a change in formulation parameters (here a change in the ratio API/PLGA/PVP and thus composition of the feed solution) can influence particle formation during spray drying. A differently composed feed solution can result in different feed viscosity, evaporation rate or solidification point of the compounds. These parameters might affect the distribution of the API in the formed microspheres and therefore the degree of API surface coverage. This is illustrated by the Peclet number (Pe) which is used to predict compound distribution of the API during the particle formation process (equation 4).

$$Pe_i = \kappa / 8D_i \quad (4)$$

In this equation the evaporation rate is represented by κ and D_i stands for the diffusion coefficient of solute i . This formula clearly indicates how a change in evaporation rate might

influence API distribution. Evaporation rate can be influenced by a varying feed composition as the affinity between solvent-polymer and solvent-drug molecules influences the evaporation rate. The extent of this influence will depend on the amount of polymer or drug molecules (with affinity for the solvent) present in solution (24). The potential influence of feed viscosity on API distribution and (surface coverage) is illustrated by the Stokes-Einstein equation which pinpoints the different parameters that influence the diffusion coefficient of a compound (equation 5).

$$D = k_B T / 6\pi\eta r \quad (5)$$

In this equation D is the diffusion coefficient, r the globular radius, T the absolute temperature and η the viscosity of the solution. k_B is the Boltzmann constant.

The higher the concentration of a compound in the feed solution, the closer it will be to its solubility limit and the faster it will reach the solidification point during the particle formation process. This possible difference of solute deposition time might also influence the spatial distribution of the API (25).

The lack of substantial differences in microspheres size and morphology (Fig. 2) when comparing the three model formulations indicates that differences in formulation parameters did not influence particle size and morphology.

In addition to influencing the particle formation process, changing the ratio of the three components might result in different mixed phases each displaying different solubility of the API and again a different distribution of the API in the spray-dried microspheres.

CONCLUSIONS

This study demonstrated how a combination of (M)DSC and the surface analysing techniques ToF-SIMS and AFM offer synergistic benefits for the characterisation of the phase behaviour and drug distribution of ternary solid dispersions (API/PLGA/PVP).

MDSC showed that the investigated formulations consisted of two mixed phases, a PLGA-rich phase and a PVP-rich phase, in which the API is present as a glass solution. ToF-SIMS informed on the spatial composition of the ternary solid dispersions: the PLGA-rich phase covers the surface of the microspheres, the PVP-rich phase is situated underneath. The degree of API surface coverage varies for the different formulations but is not in agreement with the bulk API concentration. AFM imaging and mechanical mapping coupled nanoscale spatial information about the microsphere surface to these findings, indicating structural and compositional heterogeneity in the 20 wt% API samples (compared to 10 wt% and 30 wt% API samples), which was consistent with their higher than expected surface coverage of API.

Interestingly, the distribution of the API in the ternary solid dispersions depended on formulation parameters. The extent of API surface coverage and therefore the distribution of the API over both polymeric phases differed significantly for the three formulations. As the location of the API in the microspheres might significantly influence the performance of the formulation (release behaviour and physical stability) insight into how formulation and process parameters influence the spatial distribution of the drug in these ternary solid dispersions would allow rational design of control release profiles and stability performance.

ACKNOWLEDGMENTS

Dr. Matthew Piggott (ISAC, Nottingham, United Kingdom) is acknowledged for coordinating the AFM experiments.

REFERENCES

1. Janssens S, Van den Mooter G. Review: physical chemistry of solid dispersions. *J Pharm Pharmacol.* 2009;61(12):1571–86.
2. Van den Mooter G. The use of amorphous solid dispersions: A formulation strategy to overcome poor solubility and dissolution rate. *Drug Discov Today Technol.* 2012;9(2):e71–e174.
3. Leuner C, Dressman J. Improving drug solubility for oral delivery using solid dispersions. *Eur J Pharm Biopharm.* 2000;50(1):47–60.
4. Vasconcelos T, Sarmiento B, Costa P. Solid dispersions as strategy to improve oral bioavailability of poor water soluble drugs. *Drug Discov Today.* 2007;12(23-24):1068–75.
5. Vo CL-N, Park C, Lee B-J. Current trends and future perspectives of solid dispersions containing poorly water-soluble drugs. *Eur J Pharm Biopharm.* 2013;85(3 Pt B):799–813.
6. Kalogeras IM. A novel approach for analyzing glass-transition temperature vs. composition patterns: application to pharmaceutical compound+polymer systems. *Eur J Pharm Sci.* 2011;42(5):470–83.
7. Gordon M, Taylor JS. Ideal copolymers and the second-order transitions of synthetic rubbers. i. non-crystalline copolymers. *J Appl Chem.* 1952;2(9):493–500.
8. Meeus J, Chen X, Scurr DJ, Ciarnelli V, Amssoms K, Roberts CJ, et al. Nanoscale surface characterization and miscibility study of a spray-dried injectable polymeric matrix consisting of poly(lactic-co-glycolic acid) and polyvinylpyrrolidone. *J Pharm Sci.* 2012;101(9):3473–85.
9. Meeus J, Scurr DJ, Amssoms K, Davies MC, Roberts CJ, Van den Mooter G. Surface characteristics of spray-dried microspheres consisting of PLGA and PVP: relating the influence of heat and humidity to the thermal characteristics of these polymers. *Mol Pharm.* 2013;10(8):3213–24.

10. Rafati A, Boussahel A, Shakesheff KM, Shard AG, Roberts CJ, Chen X, et al. Chemical and spatial analysis of protein loaded PLGA microspheres for drug delivery applications. *J Control Release*. 2012;162(2):321–9.
11. Scoutaris N, Hook AL, Gellert PR, Roberts CJ, Alexander MR, Scurr DJ. ToF-SIMS analysis of chemical heterogeneities in inkjet micro-array printed drug/polymer formulations. *J Mater Sci Mater Med*. 2012;23(2):385–91.
12. Kreye F, Hamm G, Karrouf Y, Legouffe R, Bonnel D, Siepmann F, et al. MALDI-TOF MS imaging of controlled release implants. *J Control Release*. 2012;161(1):98–108.
13. Weuts I, Van Dycke F, Voorspoels J, De Cort S, Stokbroekx S, Leemans R, et al. Physicochemical properties of the amorphous drug, cast films, and spray dried powders to predict formulation probability of success for solid dispersions: etravirine. *J Pharm Sci*. 2011;100(1):260–74.
14. Lauer ME, Siam M, Tardio J, Page S, Kindt JH, Grassmann O. Rapid assessment of homogeneity and stability of amorphous solid dispersions by atomic force microscopy—from bench to batch. *Pharm Res*. 2013;30(8):2010–22.
15. Lauer ME, Grassmann O, Siam M, Tardio J, Jacob L, Page S, et al. Atomic force microscopy-based screening of drug-excipient miscibility and stability of solid dispersions. *Pharm Res*. 2011;28(3):572–84.
16. Qi S, Moffat JG, Yang Z. Early stage phase separation in pharmaceutical solid dispersion thin films under high humidity: improved spatial understanding using probe-based thermal and spectroscopic nanocharacterization methods. *Mol Pharm*. 2013;10(3):918–30.
17. Alsteens D, Dupres V, Yunus S, Latgé J-P, Heinisch JJ, Dufrêne YF. High-resolution imaging of chemical and biological sites on living cells using peak force tapping atomic force microscopy. *Langmuir*. 2012;28(49):16738–44.
18. Adamcik J, Berquand A, Mezzenga R. Single-step direct measurement of amyloid fibrils stiffness by peak force quantitative nanomechanical atomic force microscopy. *Appl Phys Lett*. AIP Publishing; 2011;98(19):193701.
19. Paragkumar N T, Edith D, Six J-L. Surface characteristics of PLA and PLGA films. *Appl Surf Sci*. 2006;253(5):2758–64.
20. Van den Mooter G, Wuyts M, Blaton N, Busson R, Grobet P, Augustijns P, et al. Physical stabilisation of amorphous ketoconazole in solid dispersions with polyvinylpyrrolidone K25. *Eur J Pharm Sci*. 2001;12(3):261–9.
21. Janssens S, De Zeure A, Paudel A, Van Humbeeck J, Rombaut P, Van den Mooter G. Influence of preparation methods on solid state supersaturation of amorphous solid dispersions: a case study with itraconazole and eudragit e100. *Pharm Res*. 2010;27(5):775–85.

22. Tobyn M, Brown J, Dennis AB, Fakes M, Gao Q, Gamble J, et al. Amorphous drug-PVP dispersions: application of theoretical, thermal and spectroscopic analytical techniques to the study of a molecule with intermolecular bonds in both the crystalline and pure amorphous state. *J Pharm Sci.* 2009;98(9):3456–68.
23. Janssens S, Nagels S, Armas HN de, D’Autry W, Van Schepdael A, Van den Mooter G. Formulation and characterization of ternary solid dispersions made up of Itraconazole and two excipients, TPGS 1000 and PVPVA 64, that were selected based on a supersaturation screening study. *Eur J Pharm Biopharm.* 2008;69(1):158–66.
24. Wan F, Bohr A, Maltesen MJ, Bjerregaard S, Foged C, Rantanen J, et al. Critical solvent properties affecting the particle formation process and characteristics of celecoxib-loaded plga microparticles via spray-drying. *Pharm Res.* 2013;30(4):1065–76.
25. Paudel A, Worku ZA, Meeus J, Guns S, Van den Mooter G. Manufacturing of solid dispersions of poorly water soluble drugs by spray drying: formulation and process considerations. *Int J Pharm.* 2013;453(1):253–84.